Investigating the Fate of Mg-bearing Calcium Carbonates During Early Diagenesis

By

Zijie Gao
B.E., China University of Petroleum, Beijing, 2019

Submitted to the graduate degree program in Geology and the Graduate Faculty of the University of Kansas in partial fulfillment of the requirements for the degree of Master of Science.

Chair: Jennifer A. Roberts

Robert H. Goldstein

J. Douglas Walker

Date Defended: 19 November 2021

The thesis committee for Zijie Gao certifies that this is the approved version of the following thesis:

Investigating the Fate of Mg-bearing Calcium Carbonates During Early Diagenesis

Chair: Jennifer A. Roberts

Date Approved: 29 November 2022

Abstract

The formation of dolomite at low temperature (<80ºC) is uncommon in modern environments, however dolomite is abundant in the geologic record. The paradox between the scarcity of modern dolomite and abundance in ancient dolomite has been of long-term interest to geologists. Further, because dolomite comprises many prolific carbonate reservoirs, there are practical needs for understanding dolomite formation as it benefits petroleum exploration and development. Dolomite abundance in geologic history also reflects the secular variation of seawater through time and is a key mineral in probing past change in climate.

This study investigates whether dolomite can form from seawater in the presence of carboxylated organic matter (COM), and if the presence of COM further facilitates Mg incorporation into calcium carbonates under conditions that approximate early diagenesis and burial. The study compares Mg-incorporation in carbonate precipitated from a solution with the composition of an idealized Silurian seawater in the presence of functionalized (-COOH) organic matter followed by moderate increases in temperature (T) and pressure (P), typical of diagenesis. Three series of experiments were conducted to explore carbonate precipitation at surface conditions (T=40°C, and P=15 psi), followed by rapid sedimentation and burial during early diagenesis (T=40°C, and P=160 psi, 200 psi, 550 psi and 900 psi), and simulated diagenesis (calculated based on thermobaric gradient 1°C/122 psi; T=40°C, 40.5°C and 47°C; P=100 psi, 160 psi and 900 psi).

High Mg-calcite (mol% $MgCO_3$ ~ 11.5%) and aragonite were identified by XRD in all the vessels after incubation at surface conditions (T=40°C, and P=15 psi). As pressure increased apparent dissolution of calcite and spherulitic aragonite was observed based on analysis by SEM. During the simulation of diagenesis (additional increases in pressure and temperature), saturation indices

for carbonate minerals increased, but mol%$MgCO_3$ of calcite slightly decreased. Regrowth of calcite and new fabric of aragonite were observed under SEM, suggesting possible reprecipitation. Generally, there were few differences in bulk fluid geochemistry and mol%$MgCO_3$ of calcite precipitates between experimental and control vessels, which is probably due to the slow incorporation rate and the short incubation time (4 months). However, amorphous calcium carbonates nucleated on the surface of COM exhibited solid Mg:Ca ratios slightly larger than calcite that precipitated homogeneously from solution. This suggests that COM may facilitate Mg incorporation into calcite but under experimental conditions in this study, does not facilitate detectable dolomite nucleation nor formation.

Aside from COM, the effect of temperature and pressure on carbonate precipitation are also investigated here. Based on Phreeqc modeling of Silurian seawater composition, the saturation indices (SIs) of calcite, aragonite and dolomite increase with increasing temperature (< 65°C), and slightly decrease with increasing pressure.

While detectable dolomite was not formed in experiments that simulated precipitation under sea surface conditions nor during subsequent simulated diagenesis, changes in mol%$MgCO_3$ of calcite was observed as a function of pressure and COM. While pressure may play a role in the incorporation of Mg into the calcite structure, it is not clear from this study that its effect is large. Given adequate time for nucleation and precipitation, however, which may not have occurred due to the brevity of the experimental protocol, it is hypothesized that high Mg-calcite or dolomite is most likely formed through COM-mediated processes.

Acknowledgements

I would like to thank my advisor, Dr. Jennifer Roberts, for her continuous assistance at every stage of this project. She taught me how to define a scientific problem, design experiments, write a funding proposal, interpretate data, compare that data with literature, write and summarize a research project, which helped me become a professional researcher. Thanks to my other two committee members Dr. Goldstein Roberts and Dr. Doug Walker for discussion and providing insights of this research. Thanks to Dr. David Fowle for supporting me in building the enclosure and other lab activities. Thanks to my lab colleague Bryan Rodriguez-Colon for training me in every detail of batch experiments and elemental analysis. Especially thanks to Bruce Barnett for helping me with many technical difficulties I encountered when setting up the Parr Pressure reactor. Thanks to the staff at the University of Kansas, Department of Geology, for their warm help and support.

I would also like to thank my parents, Xiaolin and Guiming, who always support my ideas and encourage me to realize them bravely. I feel confident to deal with every challenge as long as I know they support me. Thanks to my friends Jie Shen, Luoqi, Yilin, Liuzi and Xinyi, who always listen to me, encourage me and be with me during hard times.

I would like to appreciate the funding support from the Geology department, University of Kansas, Geological Society of America (GSA), Kansas Geological Foundation (KGF), and Association for Women Geoscientists (AWG).

Table of Contents

List of Figures

List of Tables

Introduction

The origin of low-temperature dolomite has been an enigma for over a hundred years. Dolomite has two origins below ~80°C, primary and secondary. Primary dolomite is formed via direct precipitation from porewater, whereas secondary dolomite is formed through the replacement of Ca^{2+} in the calcite crystal with Mg^{2+}. This process, known as dolomitization, is responsible for the largest volume of low temperature dolomite in the rock record. Due to complex subsurface conditions, the primary phase of ancient dolomites can be altered or recrystallized, after undergoing deep burial accompanied by high temperature and potential exposure to fluids.

Dolomite is abundant in the geologic record, ranging from Archaean to Holocene (Gregg et al., 2015), however its abundance is negatively correlated with age. Dolomite becomes more stoichiometric and ordered (Manche and Kaczmarek, 2021) with age. Moreover, the fluctuations in dolomite abundance closely correlate with the variations in sulfur-isotope composition and marine benthic diversity, which can reflect oceanic redox conditions (Li et al., 2021). The distribution of dolostone in the strata may also reflect secular variations in the geochemistry of seawater. The oscillations in the composition of seawater from Cambrian to Holocene are driven by the flux of mid-ocean ridge brine, river input, and seawater-driven dolomitization (Lowenstein et al., 2001). Alternatively, some researchers posit that fluid Mg:Ca ratio influences dolomitization rate (Braithwaite, 1991; Kaczmarek and Sibley, 2011; Gabellone and Whitaker, 2016; Kaczmarek and Thornton, 2017). There is also evidence that atmospheric P_{CO2}, which directly influences solution pH and, therefore, carbonate alkalinity further controls carbonate diagenesis (Gabellone and Whitaker, 2016).

Multiple studies have successfully synthesized ordered dolomite at high temperature (> 200°C) (Kaczmarek and Sibley, 2014; Kaczmarek et al., 2017; Kaczmarek et al., 2019), however,

primary dolomite is difficult to synthesize in low-temperature (<80°C) lab environments, mirroring its scarcity in modern environments. Nonetheless, with the influence of microorganisms (Vasconcelos and McKenzie, 1997; Warren, 2000; Sánchez-Román et al., 2008; Romanek et al., 2009; Qiu et al., 2017; Qiu et al., 2019) or catalytic abiotic substances, like carboxylated polystyrene spheres, polysaccharides, clay minerals, or high concentrations of dissolved methane gas (Roberts et al., 2004; Zhang et al., 2012; Roberts et al., 2013; Liu et al., 2019), dolomite has been successfully synthesized at temperatures as low as 40°C. Researchers hypothesize that these substances dehydrate the Mg^{2+} ion, which forms strong bonds with water, inhibiting its incorporation into the growing dolomite nuclei, as well as calcite, and instead favors the precipitation of aragonite (Zhang et al., 2012; Shen et al., 2014; Petrash et al., 2017).

While microbial metabolism may play a role in creating supersaturated conditions with respect to dolomite, success in synthesizing laboratory dolomite and very high Mg-calcite (VHMC; stoichiometric Mg:Ca, but calcite crystal structure; Kaczmarek et al., 2017) in the presence of microorganisms or bacteria at room temperature, is attributed to microbial surfaces and exudates. Products of microorganisms include extracellular polysaccharides (EPS and cell walls), polysaccharides, or functional groups existing on their surface. Polysaccharides can also be strongly adsorbed by Ca-Mg carbonate, which may help weaken the chemical bonding between surface Mg^{2+} ions and water molecules. This process likely lowers the energy barrier by dehydrating Mg^{2+}-water complexes, enhancing Mg^{2+} incorporation into the precipitating carbonate, and thereby promoting disordered dolomite formation (Zhang et al., 2012). Additionally, sulfate-driven anaerobic oxidation of methane (SD-AOM) can release bicarbonate and hydrogen sulfide (Lu et al., 2018) and dissolved hydrogen sulfide can help dehydrate surface Mg^{2+} ions by increasing the competence of CO_3^{2-} to bond to the Mg^{2+} because surface-H_2S interaction is weaker

compared to strong surface Mg^{2+}- water bond. Alternatively, the larger space between H_2O/H_2S and dolomite surface provide enough room for direct interaction between Mg^{2+} and CO_3^{2-} (Shen et al., 2014), promoting the precipitation of dolomite. Negatively charged clay minerals, e.g., illite and montmorillonite, can also catalyze the precipitation of proto-dolomite through binding Mg^{2+} and Ca^{2+} ions electrostatically and dehydrating metal complexes concurrently (Liu et al., 2019).

Even though modern primary dolomite is rare compared to the abundance in the Precambrian, Holocene dolomites are found worldwide in sabkha environments (Vasconcelos and McKenzie, 1997; Wright and Wacey, 2005; Bontognali et al., 2010), which is very likely primary in origin. Under near-surface conditions, dolomitization in Holocene successions generally becomes more obvious with increasing depth, e.g., on western Andros Island, Bahamas, as soft sediments lithified progressively, the concentration of dolomite increases accordingly (Shinn and Ginsburg, 1964). In addition, modern dolomite in Los Roques N.P., Venezuelan Caribbean Sea, becomes more stoichiometric with increasing burial (Petrash et al., 2017). Nevertheless, uncertainty remains as to how proto-dolomite stabilizes to partially ordered dolomite. Or more generally, how modern near-surface dolomite formed, especially island dolomite, which has not been subjected to deep burial diagenesis (Ren and Jones, 2018).

While many studies have documented the precipitation of low temperature dolomite as influenced by Mg:Ca ratio, alkalinity and pH of parent solutions, availability and catalytic property of nucleation sites, few have documented the influence of changes in temperature and pressure typical of early diagenesis after precipitates form. This study furthers work on laboratory synthesis of dolomite at low temperature to explore the function of slightly increased temperature and pressure on the formation of near-surface carbonates, whose parent fluid is Silurian seawater, with the existence of carbon organic matter (COM).

Materials and Methods

Batch laboratory experiments were used to investigate the role of carboxylated organic matter on carbonate mineral precipitation with increasing pressure and small increases in temperature. Fluids containing carboxylated organic matter (COM) were incubated at 40°C for 121 days and compared to control experiments without COM. At the end of the first incubation period fluids and solids were then transferred to vessel and exposed to increasing pressure consistent with burial along a thermobaric gradient typical of modern carbonate platforms. Changes in mineralogy, mineral chemistry, and fluid chemistry were monitored to explore the effect of pressure on COM-nucleated carbonate minerals. As shown in Figure 1, three series of experiments were conducted to explore the carbonate precipitation at Silurian surface conditions (Series 1), rapid sedimentation and burial during early diagenesis (Series 2), and simulated normal diagenesis (Series 3).

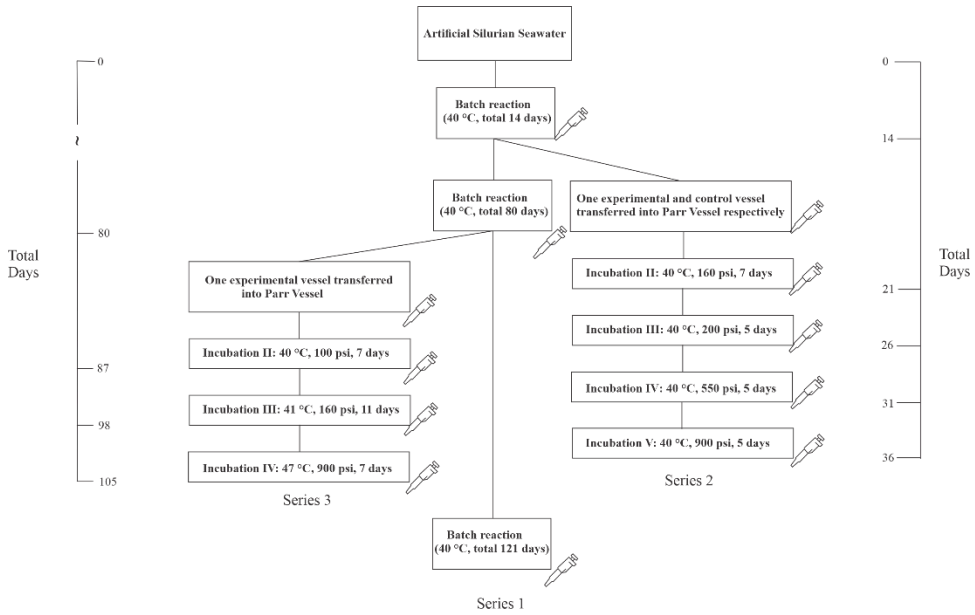

Figure 1 Experimental flowchart

Carbonate Precipitation Simulated at Surface Conditions

Fluids with a composition that approximate geochemical conditions in Silurian seawater (e.g., Lowenstein et al., 2001; Roberts et al., 2013) were made from stock powders. To allow complete dissolution, two stock reagents were prepared in the same volume of deionized water; $MgCl_2$, $CaCl_2$ and NaCl to concentrations of 96, 70, and 890 mmol L^{-1}, respectively, and Na_2CO_3, Na_2SO_4 to concentrations of 4.8 and 22 mmol L^{-1} respectively. The two stock reagents were mixed to final concentrations (Table 1) and bubbled with CO_2 to a final pH of 8.2. Solutions were then dispensed into 16, 100 ml batches in sealed 120 ml borosilicate serum bottles. Half of these were experimental vessels, in which a bulk concentration of COM with 10^{12} $RCOO^-$ L^{-1} was achieved by adding 1.2 μL 0.82-μm diameter polystyrene spheres with a $RCOO^-$ density of 796 ueq g^{-1} (Bangs Laboratory, Inv# L100616B). In contrast, the remaining sixteen batches served as control vessels, which contained no polystyrene spheres. Both the batches with and without COM were capped, and carbonate minerals were allowed to form and evolve with gentle agitation in the dark at 40°C for 30 days in an Innova 4230 refrigerated incubator and shaker (New Brunswick Scientific). Each pair of experimental and control vessels were incubated for the same time period, and when opened, their fluid and solids were analyzed at 1, 2, 5, 10, 15, 20, 25, 30, 80 and 121 d.

Effect of Pressure on carbonate recrystallization

At incubation day 14, one experimental batch or one control batch was transferred into the Parr Reactor and then sealed. The operations of setting temperature and pressure were the same as above. Batches went through four incubation steps with temperature fixed at 40°C. The pressures of Incubation I, II, III, IV were set as 160 psi, 200 psi, 550 psi, and 900 psi, respectively. At the

end of each incubation step, 30 ml solutions were sampled by pipet for analysis, as shown in Figure 2. Aqueous geochemistry and solids were characterized for each sample.

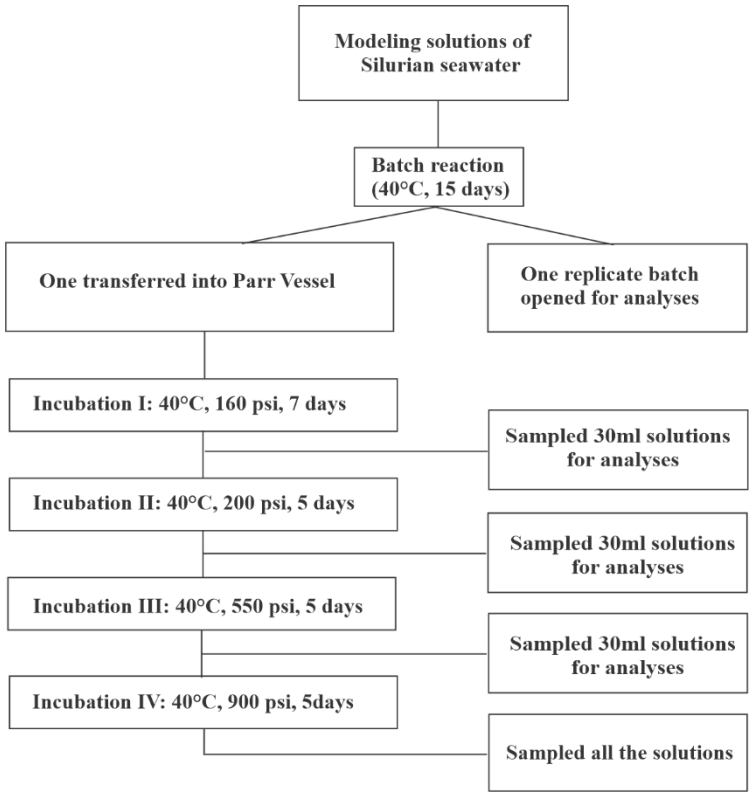

Figure 2 Schematic of varied pressure incubation at 40 °C

Experimentally simulated diagenesis

At incubation day 80, one 100 ml experimental batch was transferred into the 300 ml stainless steel vessel of a Parr Mini Bench Top Reactor 4560 in the University of Kansas Geomicrobiology Laboratory and sealed. The reactor temperature was adjusted and maintained internally, while the pressure was adjusted under an N_2 atmosphere. The batches were reacted under increasing pressure and temperature to approximate early diagenesis and burial using a geothermal gradient of 2.5ºC/100 m and 2.95 psi m^{-1} (Nwozor and Yardley, 2015), representing

the 3 to 5 kilometers below ground surface in stable continental crust (Arndt, 2011). The solutions and precipitates underwent three incubation steps to model the early diagenesis environment as shown in Figure 3. It was assumed that system would react and trend toward equilibrium in the temperature-only incubation, and mineral equilibria would shift quickly in response to higher pressure conditions. Briefly, the batches were incubated at 40ºC and 100 psi for 7 days, to model the general near-surface burial (depth ca 30 m). The second incubation step was repeated at an increased temperature 41ºC and pressure of 160 psi to model a slightly deeper burial environment (depth ca 50 m) for 11 days. The last incubation step was conducted at the temperature of 47.5ºC and pressure of 900 psi to model the depth of 300m for 7 days. At the end of each incubation, the vessel was opened and 30 ml was sampled and analyzed for mineralogy and geochemistry. After sampling, the vessel was closed and temperature and pressure were adjusted to the set value of the next incubation.

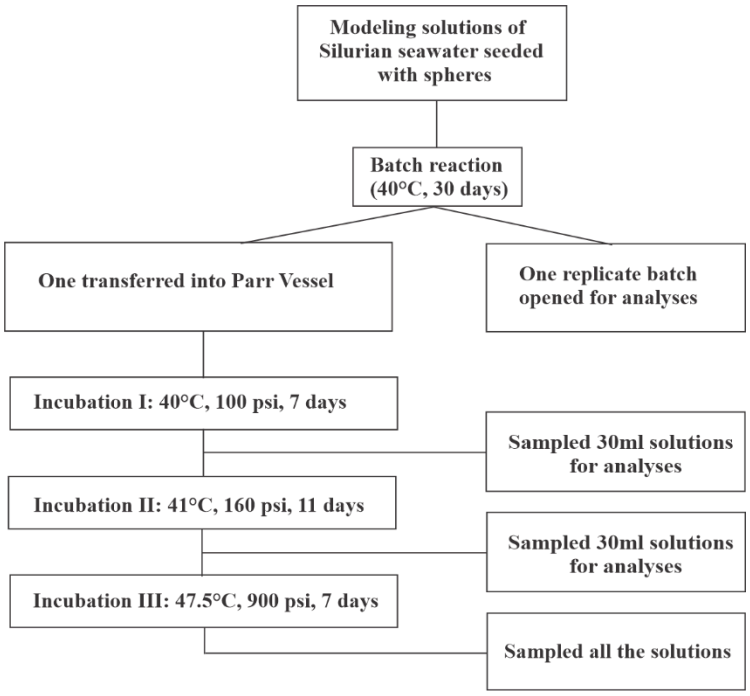

Figure 3 Schematic of experimentally-simulated diagenesis

After turning on the heating element, temperature was gradually increased from room temperature (25°C) to each set temperature (40, 41, 47.5°C) using the Parr 4848 Reactor Controller. Temperature adjustments required ~20 minutes to stabilize. Pressure was controlled using an N_2 tank whose maximum pressure was 2500 psi. The set pressure (100, 160, 900 psi) was achieved within seconds using the tank regulator. The reactor pressure gauge was used to verify the pressure inside the vessel. The Parr Reactor was purged with N_2 before the valves were closed and the vessel was pressurized. The solution inside the Parr vessel was stirred continuously during incubation using an internal magnetic stirrer whose rate was 50 rpm.

Aqueous Geochemistry

The aqueous geochemistry of the artificial Silurian seawater is given in Table 1. After each incubation step, batches were analyzed for pH, alkalinity, and cations. Solids were filtered (0.42 μm) and rinsed with deionized water and then air-dried for 24 h. The pH of the solutions was measured by a calibrated electrode (Accumet) and a pH meter (Thermo Scientific).

Fluid alkalinity was determined on a 25 mL sample using a Metrohm 807 Dosing Unit in the University of Kansas Geomicrobiology Laboratory using an end-point seeking method and a titrant of 0.1N HCl (Brezonik and Arnold, 2011).

Charge balance (Cations - Anions) / (Cations + Anions) (Freeze and Cherry, 1979) and saturation indice ($SI=\log[\text{ion activity product}/K_{sp}]$) were calculated by Phreeqc Interactive 3.6.2-15100 (Parkhurst and Appelo, 1999). Concentrations of dissolved ions, pH, temperature and pressure were input. Charge balance, activity values, and mineral saturation indices for dolomite, calcite and aragonite were calculated using the phreeqc.dat database.

Table 1 Composition of artificial Silurian seawater

Silurian Seawater Composition	(mmol L^{-1})
Na^{+}	445
Mg^{2+}	48
Ca^{2+}	35
CI^{-}	571
SO_4^{2-}	11
HCO_3^{-}	2.4
pH	8.2
R-COO− (0.82μm)	$5.1*10^{12}$
Salinity	38.5 ppm
SI_Dolomite	3.21
SI_Calcite	1.35
SI_Aragonite	1.22

Characterization of Solids

X-Ray diffraction

Precipitates were rinsed with 50 ml deionized water, air-dried, and analyzed with X-Ray diffraction using a Bruker 800 234-XRAY (9729; University of Kansas, Department of Geology). Data were collected between 5° and 70° 2θ using a step size of 0.5 seconds. Analysis of the powder XRD patterns was conducted by Materials Data JADE 7.6.6 software. Content of mol % $MgCO_3$ was calculated from XRD data, using the following formula 1:

$$y = -363.96x + 1104.05 \quad [1]$$

in which x is d[$10\bar{1}4$] dimension and y is the mol% $MgCO_3$ in Magnesian calcite (Arvidson and Mackenzie, 1999).

Electron Microscopy

Samples for analysis by Scanning Electron Microscopy were air-dried, stub-mounted, sputter-coated with 2nm Iridium and examined using an FEI Versa Three-Dimensional Dualbeam Field Emission Scanning Electron Microscope equipped with EDX detector (University of Kansas, Microscopy and Analytical Imaging Laboratory), operating at 5 KV. No additional calibration for carbonate minerals was performed on the EDX detector, so elemental signatures are interpreted as semi-quantitative.

Samples were soaked in ethanol, mounted on lacy amorphous carbon and examined using Hitachi H-8100 Transmission Electron Microscope (University of Kansas, Microscopy and Analytical Imaging Laboratory), operating at 200 KV.

Results

Carbonate Precipitation Simulated at Surface Conditions

All experiments started with incubations at 40°C and no extra pressure. The geochemical and mineralogical changes were monitored over time for experimental (containing COM) and control vessels. Materials from these experiments were then further subjected to increased pressure and temperature to discern changes in mineralogy.

Aqueous geochemistry

Charge balance for geochemical analyses for experimental and control vessels were all less than +/- 5% (Appendix A), indicating satisfactory analyses of relevant species. From the beginning of the experiment until day 121, pH decreased from a starting pH of 8.2 to 7.6 and 7.5 at day 30, to 7.5 and 7.5 at day 80, and to 7.6 and 7.5 at day 121 (experimental and control solution pH, respectively; Figure 4). In general, solution pH for both experimental and control vessels were similar, although experimental vessels were slightly higher than control vessels. For both groups of vessels, the maximum pH was achieved around 14 d, and then pH decreased and stabilized around 7.5 after 30 d.

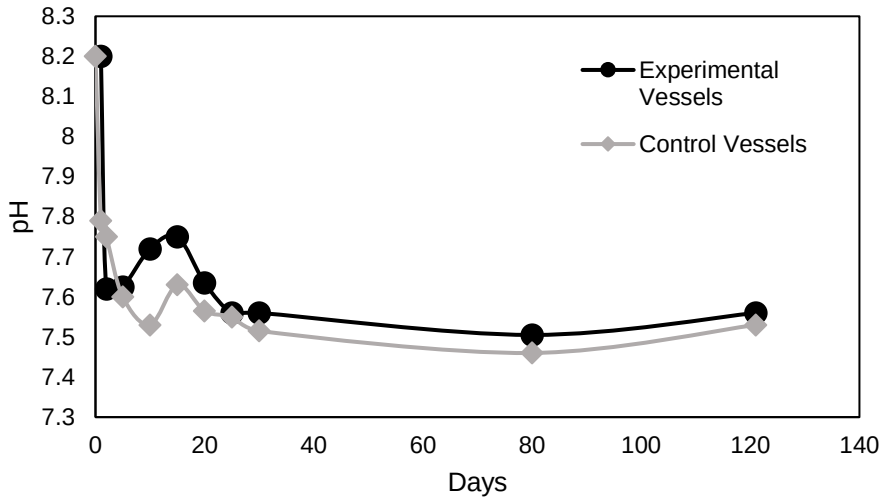

Figure 4 Change in fluid pH over time for incubations at 40°C.

Over the experiment's duration, alkalinity decreased from 2.7 mmol L^{-1} to 0.5 and 0.5 mmol L^{-1} respectively (experimental and control vessels; Figure 5). For control vessels, alkalinity increased sharply at 5 d and then decreased gradually with time. For experimental vessels, the alkalinity decreased to ~0.7 mmol L^{-1} at 15 d, and then gradually decreased to 0.5 mmol L^{-1}.

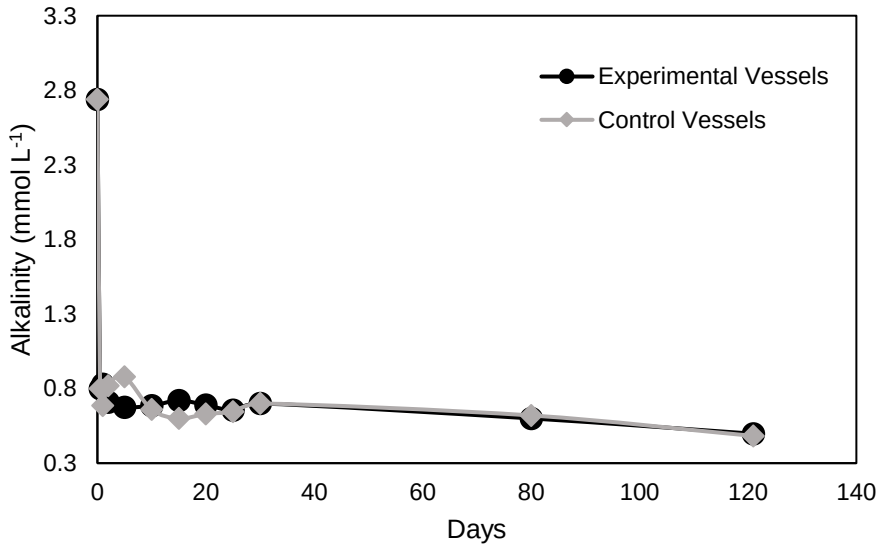

Figure 5 Change in alkalinity over time for incubations at 40 °C

The concentration of Mg^{2+} decreased from 58 mmol L^{-1} to 49 mmol L^{-1} and 50 mmol L^{-1} respectively at day 121 (experimental and control vessels; Appendix A). The concentration of Ca^{2+} decreased from 38 mmol L^{-1} to 34 mmol L^{-1} and 34 mmol L^{-1} respectively at day 121 (experimental and control vessels; Appendix A). The Mg:Ca ratio was ~1.5 for both experimental and control vessels (Figure 6). However, their pathways were slightly different before 80 d. The Mg:Ca ratio of control vessels sharply decreased at the first 10 days, and then became relatively stable, although abruptly increased at 30 d. In contrast, the Mg:Ca ratio of experimental vessels slightly fluctuated and generally decreased. The ratios of experimental and control vessels became close to each other starting from 80 d.

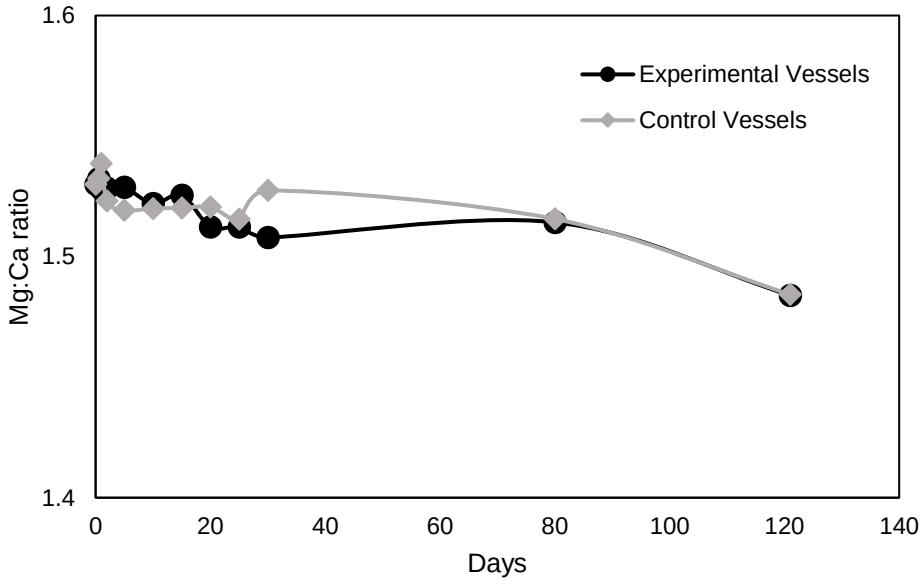

Figure 6 Change in fluid Mg:Ca over time for incubations at 40 °C

The saturation indices (SI) of aragonite, calcite, and dolomite were initially greater than 0, which means initially the solution was supersaturated with respect to all three carbonate minerals. As shown in experimental vessels, the saturation state dropped from 3.3, 1.4 and 1.3 to -2.4, -1.3

and -1.4, respectively (for dolomite, calcite, and aragonite). Changes in saturation indices of dolomite, calcite, and aragonite were correlated. In control vessels, the SIs dropped to -2.2, -1.3 and -1.4, respectively (for dolomite, calcite, and aragonite), as shown in Figure 7.

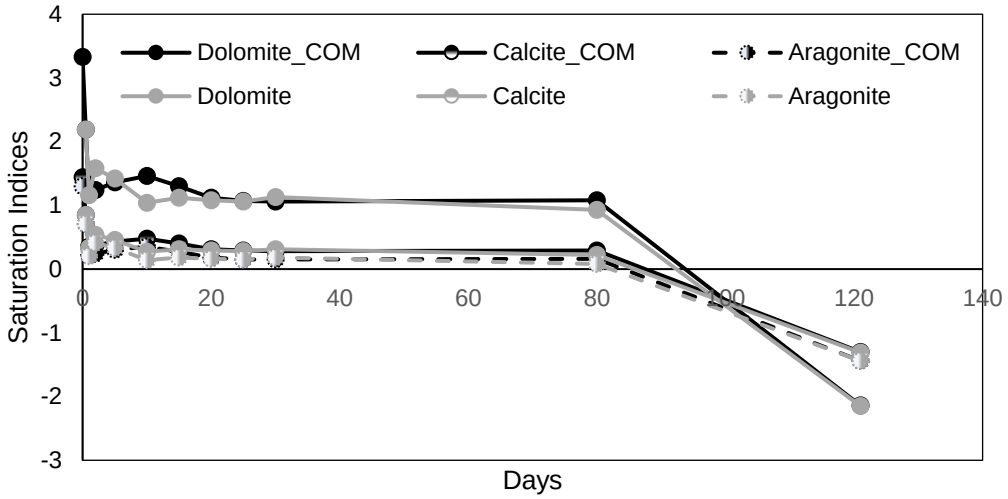

Figure 7 Change in saturation indices of dolomite, calcite and aragonite over time

However, the SIs of experimental vessels decreased gradually, versus control vessels dropped down sharply and then increased. Starting around 25 d, the dolomite SIs of experimental and control vessels were nearly identical, as were calcite and aragonite. It was estimated that the calcite and aragonite achieved equilibrium around day 90 (SI=0), and then became undersaturated.

Mineralogy

For both experimental and control groups, mineral composition was determined via analyzing the XRD pattern of the solid samples. Calcite was identified in all experimental and control vessels starting at day 1. Additionally, some smaller peaks were identified as aragonite

(Figure 8). For both experimental and control vessels, the mol% $MgCO_3$ in calcite was approximately 11.5%.

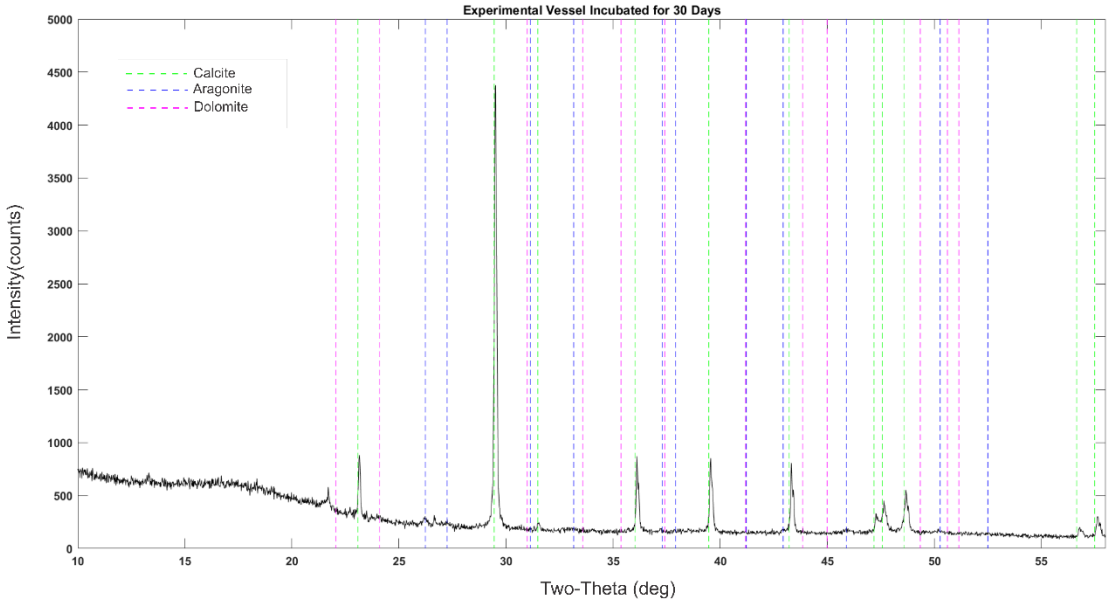

Figure 8 XRD graph of experimental vessel incubated at 40°C for 30 days

The XRD patterns of experimental and control vessels at 15 d were nearly the same. However, the calcite and aragonite peaks of experimental vessel were greater intensity than those of control vessel at 121 d (Appendix Figure A-1).

The calcite peaks of control vessel at 121 d had higher intensity than those at 15 d (Appendix Figure A-2), but the intensity of aragonite peaks stayed nearly the same. However, both the calcite and aragonite peaks from the experimental vessel at 121 d were more intense than those at 15 d (Appendix Figure A-3).

Scanning Electron Microscopy

Calcite and aragonite were identified by crystal morphology using SEM. Based on observational data, calcite was the predominant mineral, which corresponded with the results from

XRD. Two morphologies of calcite formed; subhedral and contact twin (Figure 9a). Very clear rhombohedral habit can be seen at the edge of the subhedral calcite crystals (Figure 9d), indicating undisturbed growth. In addition, aragonite exhibited two morphologies in this experiment, one is spherulitic (Figure 9b) and the other is tabular (Figure 9c). Morphologies for both minerals, as well as their abundance, did not differ between the experimental and control vessels. However, in experimental vessels, it was observed that there was a thin mineral layer on the surface of carboxyl polystyrene spheres.

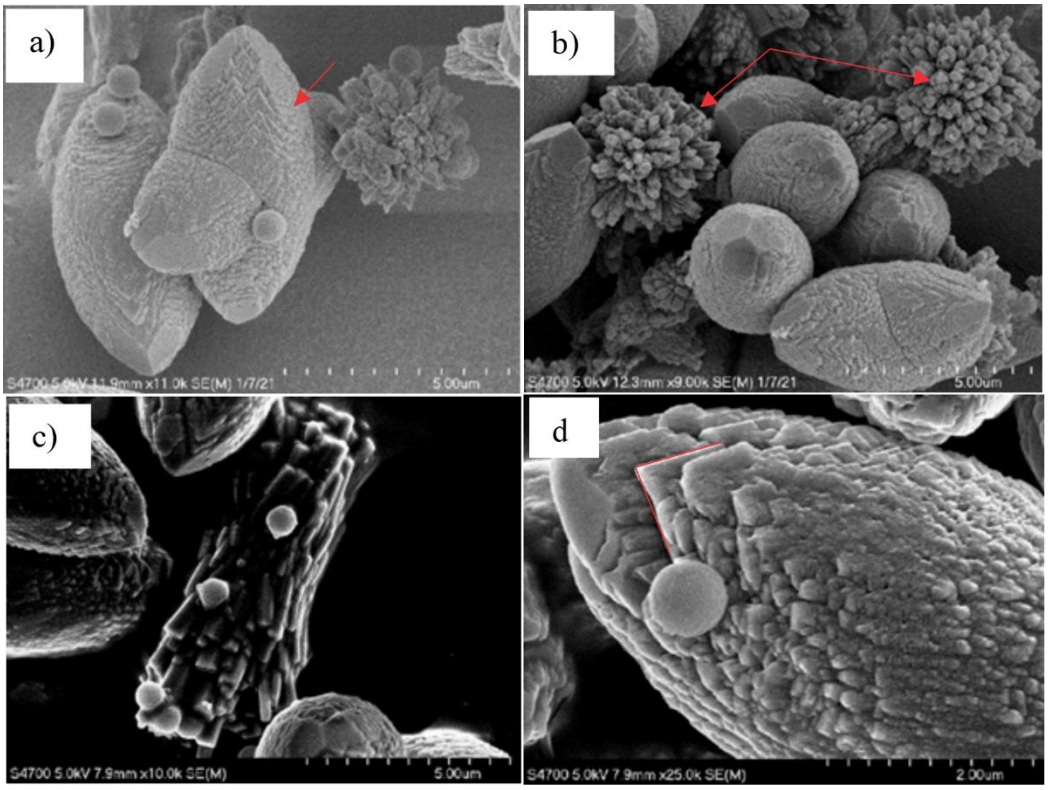

Figure 9 a) SEM image of twin calcite (red arrow) formed at 40°C, 15 psi b) SEM image of spherulitic aragonite (red arrow) formed at 40°C, 15 psi c) SEM image of tabular aragonite (red arrow) formed at 40°C, 15 psi d) SEM image of rhombohedral habit (red line)

From EDX data, it was determined that the materials on the surface of COM were calcium carbonates with little magnesium (Figure 10).

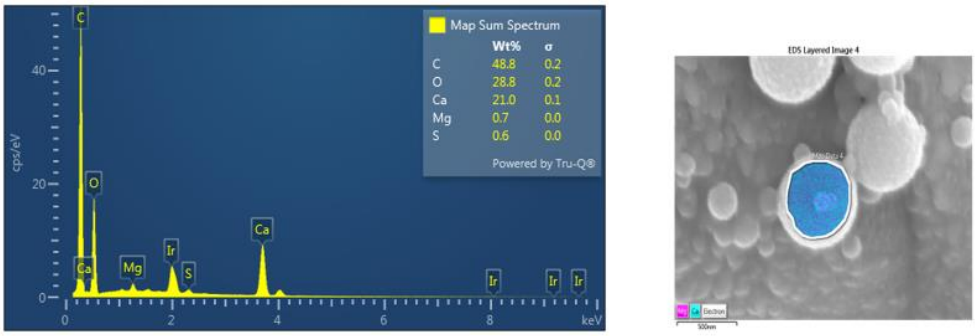

Figure 10 Elementary composition of mineral layers on the surface of COM from experiment vessel at day 14. a) Map Sum Spectrum b) EDS Layered Image

However, examination using transmission electron microscopy, revealed no crystallites on the surface of the carboxyl polystyrene sphere, so these calcium rich materials were amorphous or alternatively, Ca complexed at the surface (Figure 11).

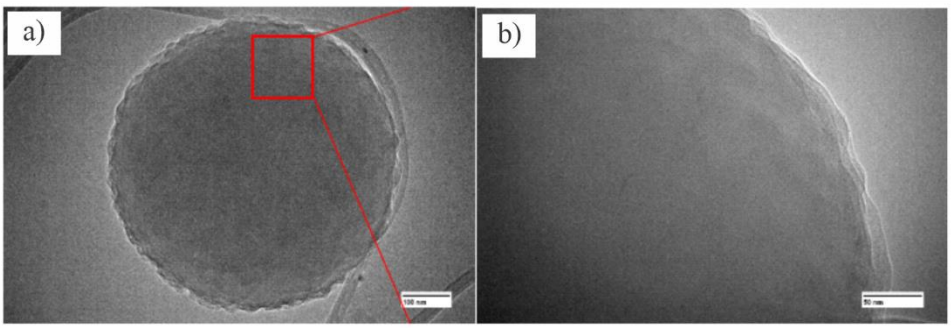

Figure 11 a) Transmission Electron Microscopy images of the mineral layers on the surface of COM b) Magnified corner of a)

After 80 days of the temperature-only incubation, the solutions and solids from one of the experimental batches were transferred into the Parr pressure reactor. Three sequential incubations (40 °C, 100 psi; 41 °C, 160 psi; 47.5 °C, 900 psi) were conducted on these materials with increased pressure and temperature (P&T).

Carbonate dissolution simulated at rapid burial during early diagenesis

Batches underwent 14 days of temperature-only incubation at 40 °C before they were transferred into the pressure reactor. Pressure was increased to 160 psi for 7 days, then to 200 psi for 5 days, then to 550 psi for 5 days, finally to 900 psi for 5 days. Temperature was held constant at 40°C through the whole experiment.

Aqueous Geochemistry

Over the course of the experiment, pH dropped from 8.2 to 7.5 at day 26 for both experimental and control vessels. After pressure was increased above 200 psi, pH increased to 7.7 and 7.9 respectively (experimental and control; Figure 12).

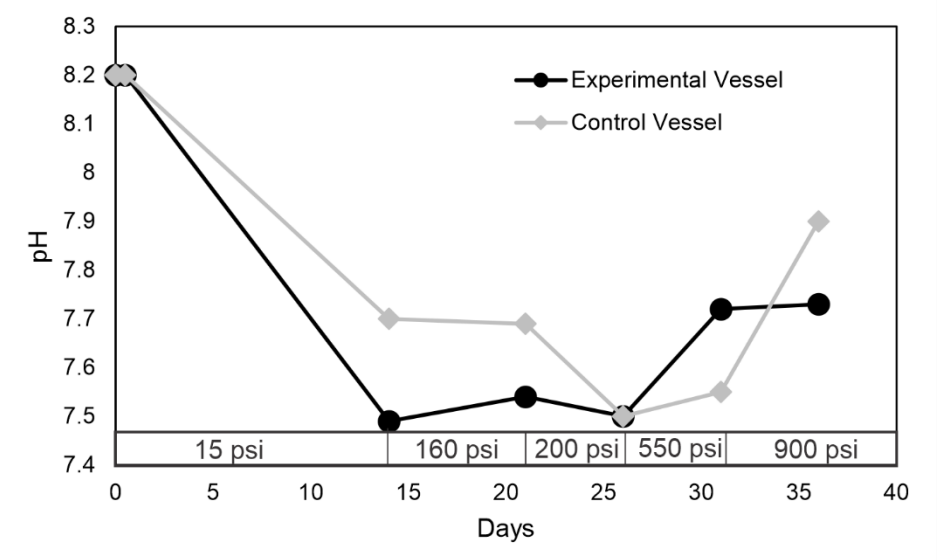

Figure 12 Change in pH over time

Starting from the day solutions were made, alkalinity decreased from 2.4 mmol L^{-1} and 2.6 mmol L^{-1} to 0.4 mmol L^{-1} respectively (experimental and control). Compared with samples extracted from the same incubation day but without pressure, increasing pressure resulted in alkalinity decreasing (Figure 13).

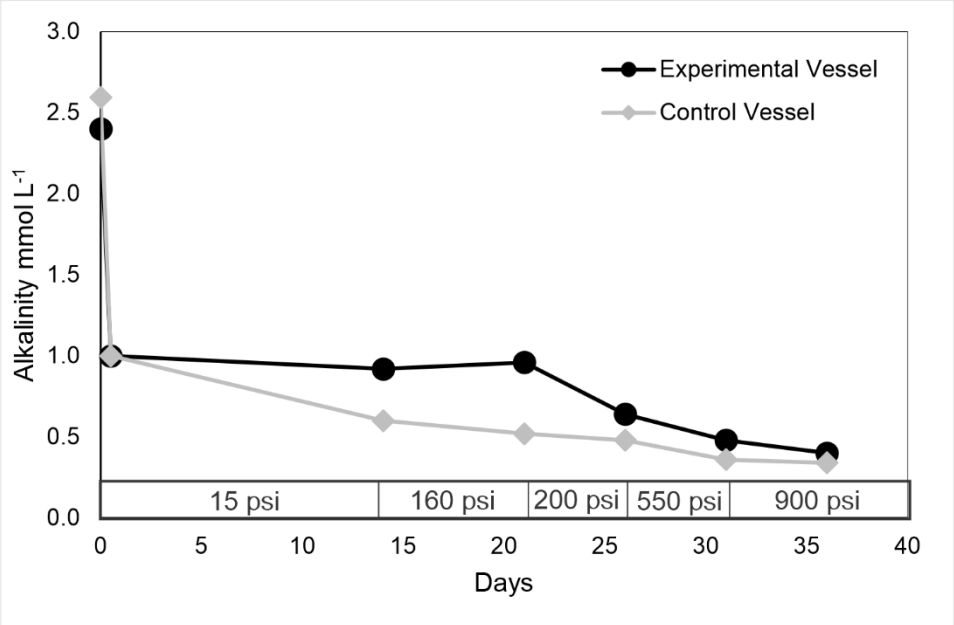

Figure 13 Change in alkalinity over time

Starting from the day 0 of experimental vessels, the concentration of Mg^{2+} and Ca^{2+} decreased from 48 mmol L^{-1} and 35 mmol L^{-1} to 42 mmol L^{-1} and 30 mmol L^{-1}, respectively. These changes occurred in the hour after the solutions were made, due to the quick precipitation when mixing stock reagents. Then, the concentration of Mg^{2+} and Ca^{2+} increased to 51 mmol L^{-1} and 36 mmol L^{-1} at day 36. Similarly, from the beginning of control vessels were made, the concentration of Mg^{2+} and Ca^{2+} quickly decreased from 52 mmol L^{-1} and 38 mmol L^{-1} to 52 mmol L^{-1} and 38 mmol L^{-1}, then increased to 53 mmol L^{-1} and 37 mmol L^{-1} at day 14, and finally decreased to 49 mmol L^{-1} and 34 mmol L^{-1} at day 36. In addition, the fluid Mg:Ca ratio stayed 1.4 all through the experiment. However, there was slightly more variation in Mg:Ca in control vessels. Starting from the beginning of the experiment, the fluid Mg:Ca ratio increased from 1.4 to 1.5 at day 20, when 160 psi had been exerted for 7 days. Then it decreased to 1.4 at day 30, and finally increased to 1.5 again at the end of the experiment(Figure 14).

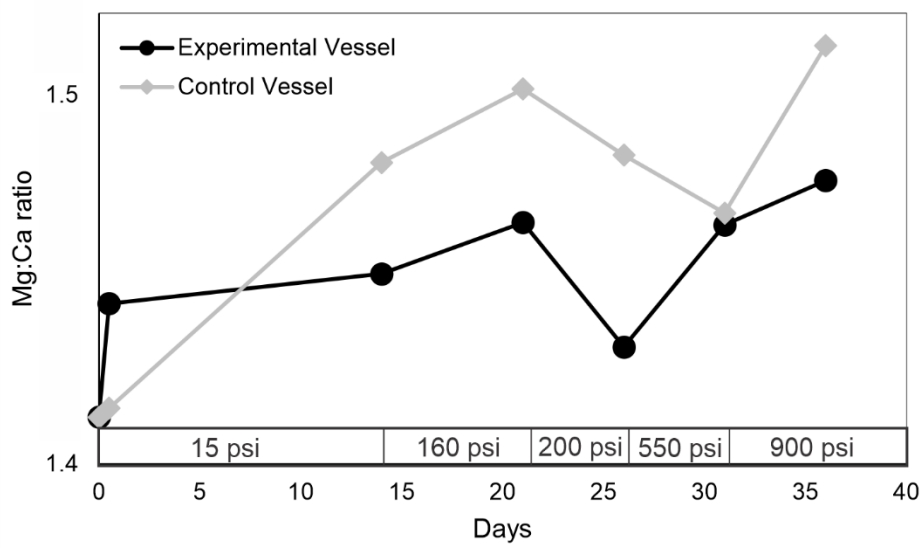

Figure 14 Change in fluid Mg:Ca over time

For both experimental and control vessels, the saturation indices of dolomite, calcite, and aragonite were positively correlated. Starting from day 0, the saturation indices of carbonate species in experimental vessels generally decreased from 3.2, 1.4 and 1.2 to 0.8, 0.16 and 0.03, respectively (dolomite, calcite, and aragonite) at day 36 (Figure 15). For control vessels, the saturation index of dolomite, calcite, and aragonite decreased from 3.3, 1.4 and 1.3 to 0.44, -0.02 and -0.15 at day 31 (pressure was set at 550 psi), at which calcite and aragonite were close to equilibrium. Then the pressure was increased to 900 psi and the saturation index slightly increased to 0.63, 0.07, and -0.06, respectively (dolomite, calcite, and aragonite).

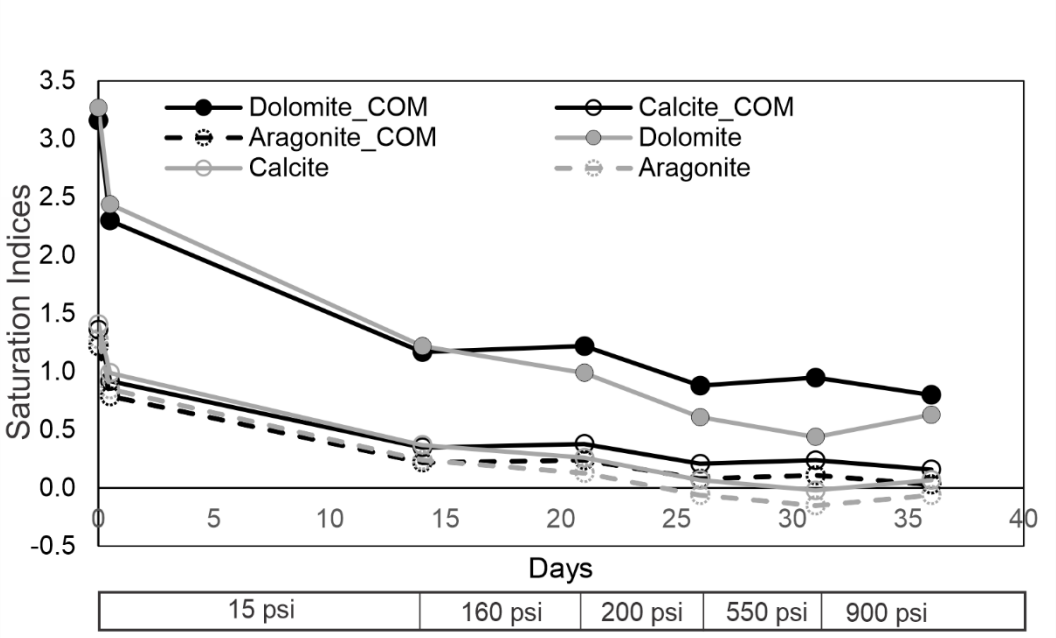

Figure 15 Saturation Indices of dolomite, calcite and aragonite over time

Minerology

For experimental vessels, peaks of calcite and aragonite at day 31, at which the pressure was set at 550 psi, were more intense than those at day 14 (Appendix Figure B-1), when pressurization began.

For control vessels (Figure 16) the intensity of calcite and aragonite peaks increased at day 31 (500 psi for 5 days) relative to the precipitations when solutions were just made (day 0.5). However, those peaks became less intense at day 36 (900 psi for 5 days).

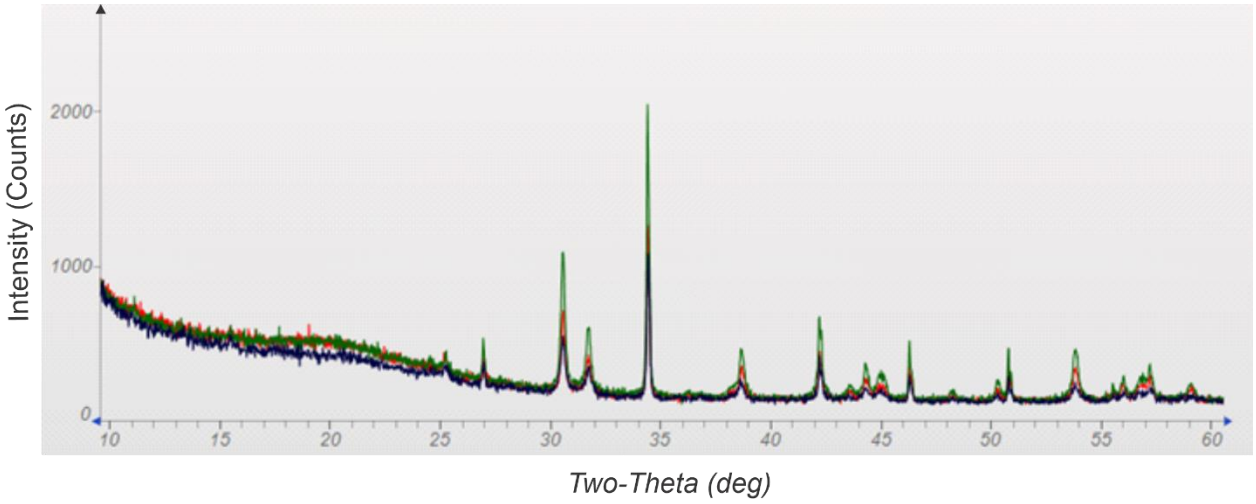

Figure 16 XRD pattern at 0.5d, 31d (green) and 36 d (red)

As observed in experimentally simulated diagenesis, spherulitic aragonite, tabular aragonite and calcite (Figure 17a). Additionally, apparent dissolution made the crystal edges of calcite and tabular aragonite rounded (Figure 17b), compared to the clear terminations observed before pressurization.

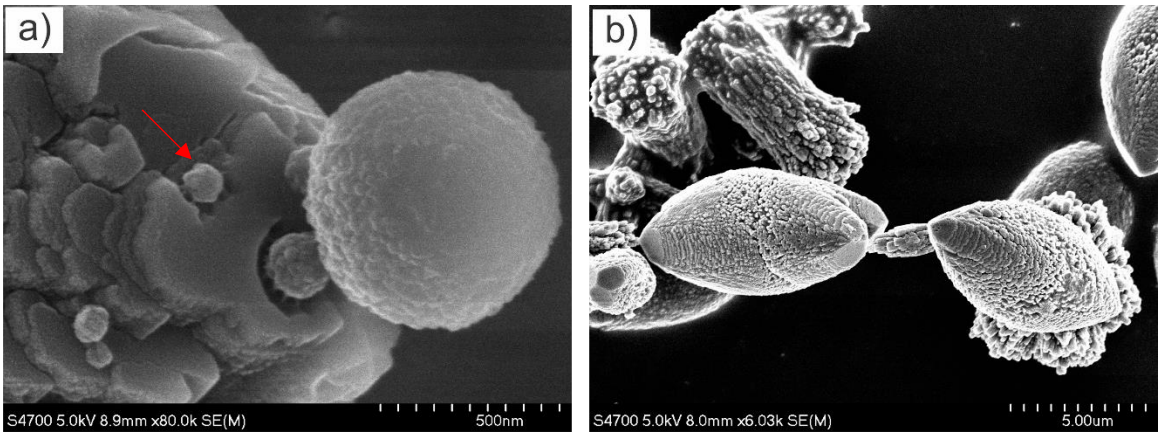

Figure 17 a) SEM image of the etching and embaying of calcite (red arrow) and COM with mineral layer(right) in experimental vessel (40 °C, 15 psi for 14 days; 160 psi for 7 days; 200 psi for 5 days; 550 psi for 5 days) b) Partially dissolved calcite and tabular aragonite

Based on the Ca and Mg wt% from EDS data, solid Mg:Ca ratios of carboxylated organic matter (COM) surfaces was compared to calcite from experimental and control vessel (Figure 18). The average solid Mg:Ca ratios of COM and calcite in experimental and control vessels were 0.059, 0.051 and 0.055, respectively. The solid ratio of COM was slightly higher than authigenic calcite, especially compared to calcite in the same batch, and less scattered. Due to a lack of carbonate-specific calibration, it cannot be verified that the measurements are different within error.

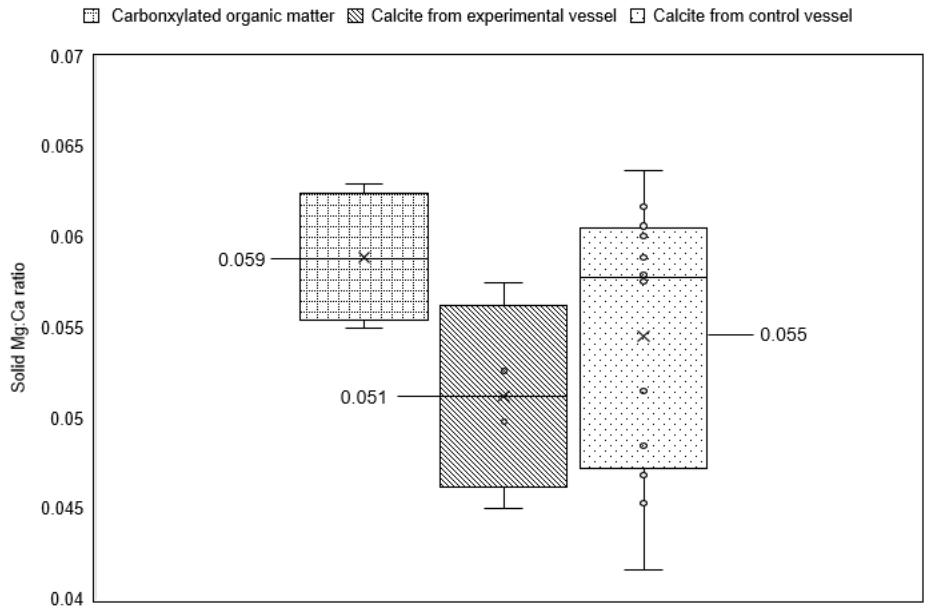

Figure 18 Box plot of the solid Mg:Ca ratio of mineral layer on COM, calcite from experimental and control vessels, calculated from EDS data.

Carbonate dissolution and reprecipitation simulated at normal diagenesis

Aqueous Geochemistry

Charge balance for geochemical analyses for the three sequential P&T incubations were all within +/- 5% (Appendix C). Starting day 0, the pH fluctuated but generally decreased until day 80. Solution pH then decreased to 7.6 at day 98 (the end of P&T incubation II), but increased to 7.9 at day 105, which was the highest pH over the experiment's duration (Figure 19). Starting

from day 80, (the day P&T incubations started) the alkalinity dropped to 0.5 mmol L^{-1} at 98 d, then further dropped to 0.4 mmol L^{-1} at day 105 (the end of P&T incubation III), which was the lowest alkalinity over the whole experiment (Figure 20).

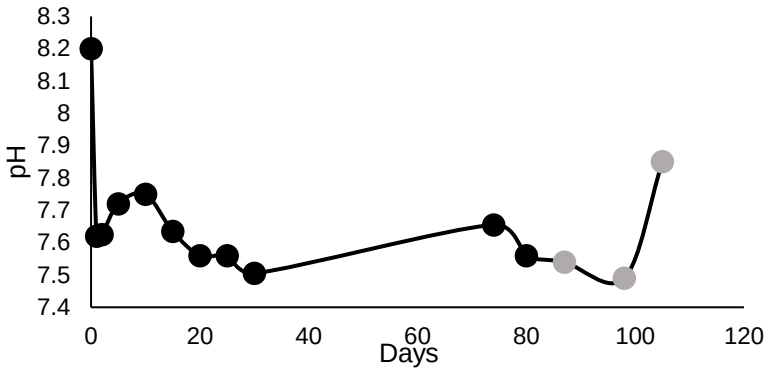

Figure 19 Change in fluid pH over time in experimental vessels (gray dots for P&T incubation)

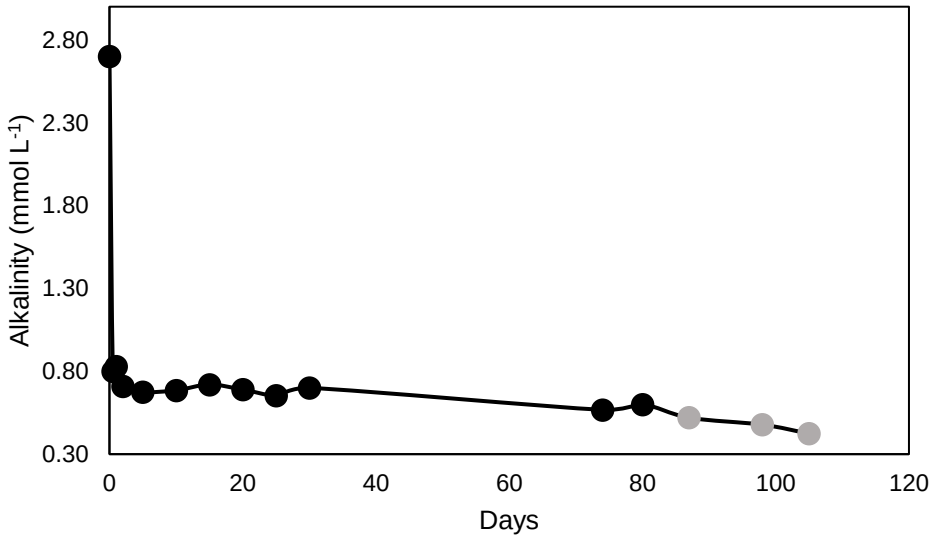

Figure 20 Change in alkalinity over time in experimental vessels (gray dots for P&T incubation)

Aqueous concentrations of Mg^{2+} and Ca^{2+} decreased to 62 mmol L^{-1} and 41 mmol L^{-1}, respectively at day 87, but then sharply increased to 71 mmol L^{-1} and 47 mmol L^{-1} respectively at

day 98, and then decreased to 67 mmol L^{-1} and 43 mmol L^{-1} respectively at day 105. The Mg:Ca ratio maintained at ~1.5 through the whole P&T incubation. As shown in Figure 21, starting from day 80 to day 98, the saturation indices of dolomite, calcite, and aragonite decreased from 1.1, 0.3 and 0.2 to 0.8, 0.1 and 0.1, respectively, which was very close to equilibrium, especially for aragonite. However, from day 98 to day 105, when the temperature and pressure were increased to 47 °C and 900 psi respectively, the saturation indices increased to 1.3, 0.4 and 0.2 (dolomite, calcite, and aragonite).

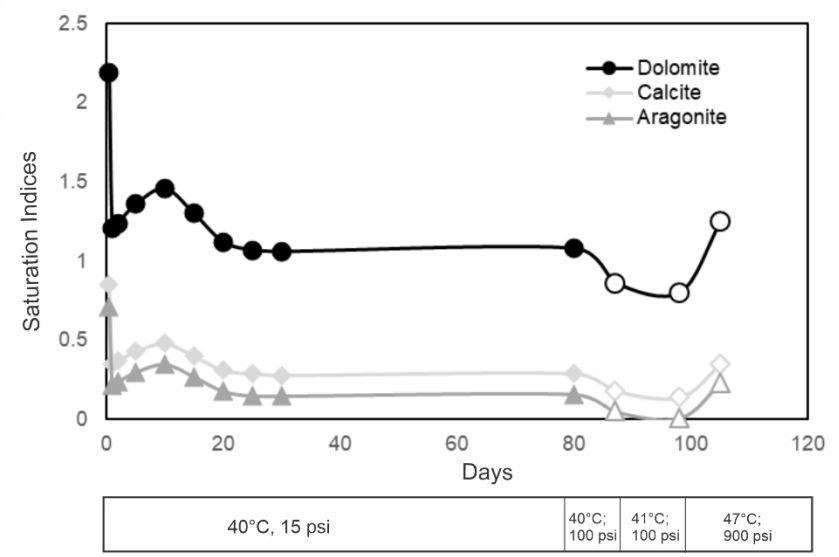

Figure 21 Saturation indices of dolomite, calcite, and aragonite (unfilled dots for P&T incubation)

Mineralogy

Similar to solid samples which experienced temperature-only incubations, the samples which were pressurized also identified as calcite-dominant with small amounts of aragonite. The mol% $MgCO_3$ in magnesian calcite before 87 d (40 °C, 100 psi) was 11.6% and slightly decreased to 11.5% after 98 d (41 °C, 160 psi).

Aragonite peaks were nearly identical to day 87, but slightly more intense in day 80 than in day 98 and day 105 (Appendix Figure C-1). The peaks of calcite were abruptly less intense from 80 days to 87 days (Appendix Figure C-2), when the pressure was first engaged in the system. At the end of P&T incubation, the intensity of calcite slightly decreased (Appendix Figure C-1).

SEM observation revealed that the precipitates formed at 40°C and 15 psi were altered by dissolution and reprecipitation after the pressure increased. Deep etching of the crystal surface observed under increased pressure is interpreted as partial dissolution of calcite (Figure 22b). In addition, the left calcite in Figure 22b intruded into the right calcite, suggesting the regrowth of the left calcite or competitive growth of calcites. In addition, a new fabric of aragonite formed, with spiky clumps that retained acicular fabric in addition to equigranular crystals (Figure 22a). Furthermore, the concentrations of Mg^{2+} and Ca^{2+} decreased, implying the ions were fixed into solids. These data support in combination that reprecipitation happened after dissolution.

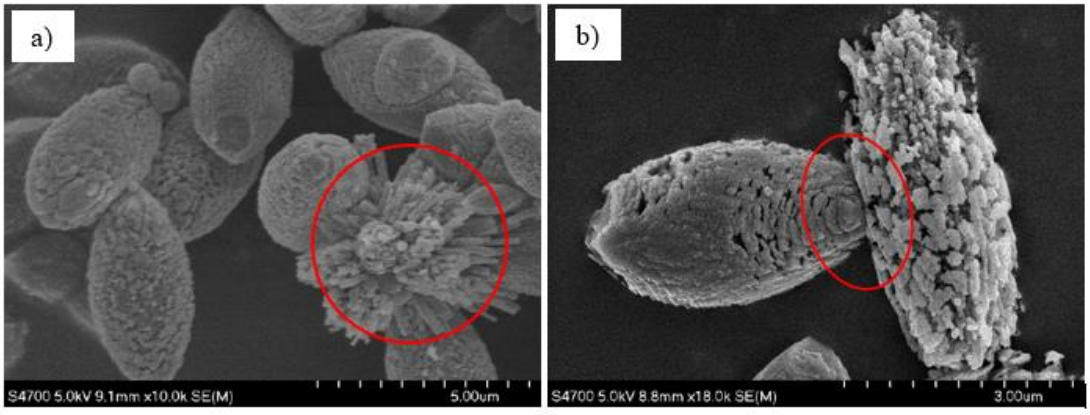

Figure 22 a) SEM of partially dissolved and recrystallized spherulitic aragonite (red circle) formed in experimental vessel (40 °C, 15 psi for 80 days; 40 °C, 100 psi for 7 days) b) Contact boundary (red circle) of recrystallized calcite(left) and partially dissolved calcite (right)

Discussion

Carbonate Precipitation Simulated at Surface Conditions

Under earth surface temperatures (40°C) and pressures (15 psi), solutions initially supersaturated with respect to dolomite, aragonite, and calcite became less supersaturated, commensurate with decreases in fluid concentrations of alkalinity and pH, indicating carbonate precipitation, which were identified as Mg-calcite and aragonite. Experimental conditions (Table 1) were designed to represent tropical near-surface conditions for seawater with compositions typical of those present during the Silurian (Brennan and Lowenstein, 2002). Modern conditions in contrast have significantly higher sodium (485 mmol L^{-1} vs. 445 mmol L^{-1}), sulfate (29 mmol L^{-1} vs. 11 mmol L^{-1}) and fluid Mg:Ca ratios (5:1 vs. 1.4:1), but lower chloride (565 mmol L^{-1} vs. 601 mmol L^{-1}) (Holland et al., 1986). Results from this study produced Ca carbonates with mol% $MgCO_3$ ranging from 11.5% to 11.6%, which falls into the upper range of mol% $MgCO_3$ of Mg calcite preserved in Silurian echinoderms (6% to 12%; Dickson, 2004), but still not very high-Mg calcite or dolomite as hypothesized. In contrast, near-stoichiometric (50.3 mol% $MgCO_3$) and well-ordered Paleogene dolomite, which was dolomitized by near-normal marine fluids, can be formed at the very early stage of diagenesis (Ryan et al., 2020). The formation of early-diagenesis Paleogene dolomite may be caused by the effect of much longer geologic time, compared to maximum four-months incubation of my experiments in this study, which compensated for the slower reaction rate under low temperature (Kaczmarek and Thornton, 2017).

Distinctive crystal habits of precipitated phases were observed with SEM, consistent with homogeneous nucleation, which are larger (>5 μm) and not associated with spheres (0.82 μm). For heterogeneous nucleation, the surface nucleation sites probably have catalytic effect on magnesium carbonate formation, (Petrash et al., 2017), by promoting inclusion of Mg into the

crystal structure (Braissant et al., 2007; Fangfu Zhang et al., 2012; Roberts et al., 2013). For experiments in this study COM was expected to facilitate dolomite formation, by binding and dewatering Mg and thus promoting nucleation of dolomite. Although dolomite was not detected with XRD, precipitate layers were observed on the surface of COM in experimental vessels, suggesting heterogeneous nucleation promoted by the COM surface. Furthermore, solid Mg:Ca ratio of COM-associated precipitate layers (0.059) is slightly larger than that of homogeneous calcite (0.051), which is consistent with previous research showing that the carboxyl-rich surface of COM can lower the energy of carbonation, making the incorporation of Mg relatively easier (Roberts et al., 2013). Nevertheless, the bulk fluid geochemistry and mol% $MgCO_3$ of solids in experimental (with COM) and control vessels (without COM), show little difference. This similarity may be a result of the short time scale of the experiments, or the size scale of more Mg-rich phases is too small to be detected. Heterogeneous nucleation still makes a difference because amorphous carbonates or Ca-rich complexes coating only form on the surface of the COM. Nonetheless, it suggests that the kinetic barrier of dolomite formation, which is due to the difficulty of dewatering Mg^{2+} and incorporating it into calcite crystal (Lippmann, 1973; Mirsal and Zankl, 1985; Fangfu Zhang et al., 2012), is hard to break under low temperature, even in the presence of COM.

Moreover, the saturation indices (SI) of dolomite, calcite and aragonite decreased to below 0, indicating the solutions went from supersaturated to undersaturated due to carbonate mineral precipitation. High Mg-calcite, defined as calcite with mol% $MgCO_3$ > 4% (Tucker and Wright, 1990), and aragonite were detected by XRD at the beginning of the experiments, implying calcium carbonate formation occurred very quickly at the beginning of the experiments. The mineralogy and calcite %$MgCO_3$ composition showed little difference over the next four-month incubation

period. Comparisons of solid Mg:Ca ratio between COM surfaces and calcite precipitates in both experimental and control vessels, reveal potentially higher accumulations of Mg on the COM surface (Figure 18). This result is similar to results from Kenward et al. (2013), which demonstrated preferential adsorption of Mg over Ca on the surface of nonmetabolizing cells and reinforces the possibility that this is a first step in nucleating Mg-bearing Ca carbonate phases.

The Role of Pressure and Temperature

In additional to fluid geochemistry, temperature and pressure control Ca carbonate polymorph (Hacker et al., 2005; Kawano et al., 2009). Generally, calcite is dominant at low temperature (<20°C) and atmospheric pressure. There are four major diagenetic settings in carbonate systems, which are marine, meteoric, evaporative, and subsurface. Meteoric and evaporative diagenetic environments are usually low temperature and low pressure. However, in marine diagenesis environments, temperature and pressure change when moving from warm surface water environments to cold shelf margins. The temperature and pressure of burial diagenetic environments progressively increases with depth (Moore and Wade, 2013).

Phreeqc modeling of artificial Silurian seawater fluids in this study (Figure 23) shows that the saturation indices of dolomite increase from 3.2 (40°C) to 3.3 (60°C), and then decreases to 1.8 at 100 °C. The saturation indices of calcite and aragonite start at 1.4 and 1.2 (40°C) respectively, achieving a maximum of 1.4 and 1.3 at 65°C, and then decrease sharply to 0.86 and 0.76 at 100°C. SI reflects the log of the saturation state of mineral. If SIs <0, dissolution is favored; if SIs =0, system is in equilibrium; if SIs >0, precipitation is favored. As shown in formula 2, K_{sp} is negatively correlated with SI, which means the higher SIs, the more soluble the compound will be

(low K_{sp}). Within the temperature range of the experiments (from 40 °C to 47 °C), the SIs of dolomite, calcite, and aragonite increase with increasing temperature.

$$SI = \log\left(\frac{IAP}{K_{sp}}\right) \quad [2]$$

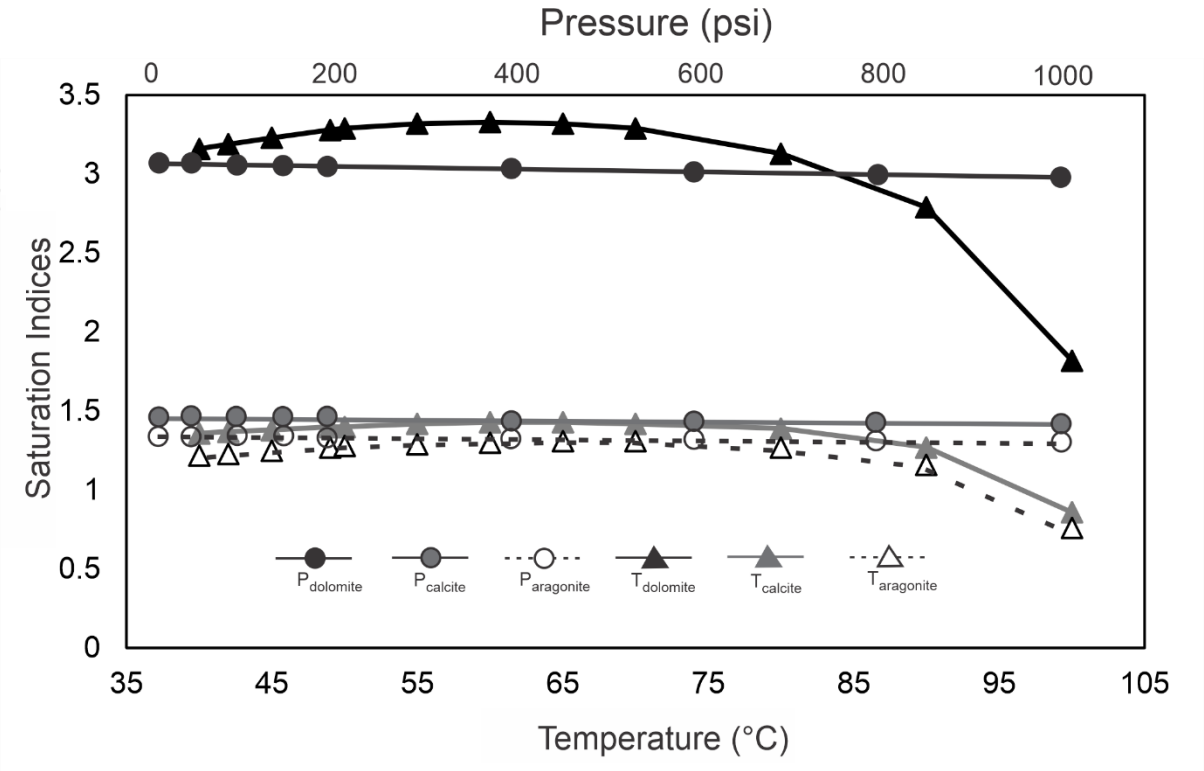

Figure 23 Saturation indices of dolomite, calcite, and aragonite of artificial Silurian seawater under varied temperature and pressure, calculated by Phreeqc. Pressure correlates to the top x-axis and temperature correlates to the bottom x-axis. P in the legends indicates the series of pressure, and T indicates that of temperature.

Additionally, if the temperature is kept at 40°C, but the pressure varies, the SIs of dolomite, calcite, and aragonite decrease with increasing pressure. Generally, dolomite is more sensitive to the changes in pressure and temperature than calcite and aragonite (Figure 23). Fluids at low temperatures but higher pressure can occur in environments in which rapid sedimentation occurs such as periplatform in Exuma Sound, Bahamas (Dix and Mullins, 1988). Alternatively, this can

occur when strata that confine fluids are capped with lower permeability sediments, such as evaporites or cemented layers, thus creating abnormal high geopressure (Moore and Wade, 2013).

In laboratory experiments in this study, temperature was kept constant at 40°C, but pressure was varied to explore the single effect of pressure on carbonate precipitation, typical of rapid sedimentation and burial. The experimental processes were designed to mimic two different geologic processes: precipitation of carbonates under shallow seawater followed by subsequent rapid burial. As shown in Figure 24, in lab experiments, carbonates firstly precipitated, and then these precipitations were partially dissolved with the increasing pressure, demonstrated by the SIs (<0), increasing concentrations of metal ions in the solutions and the dissolution evidence under SEM.

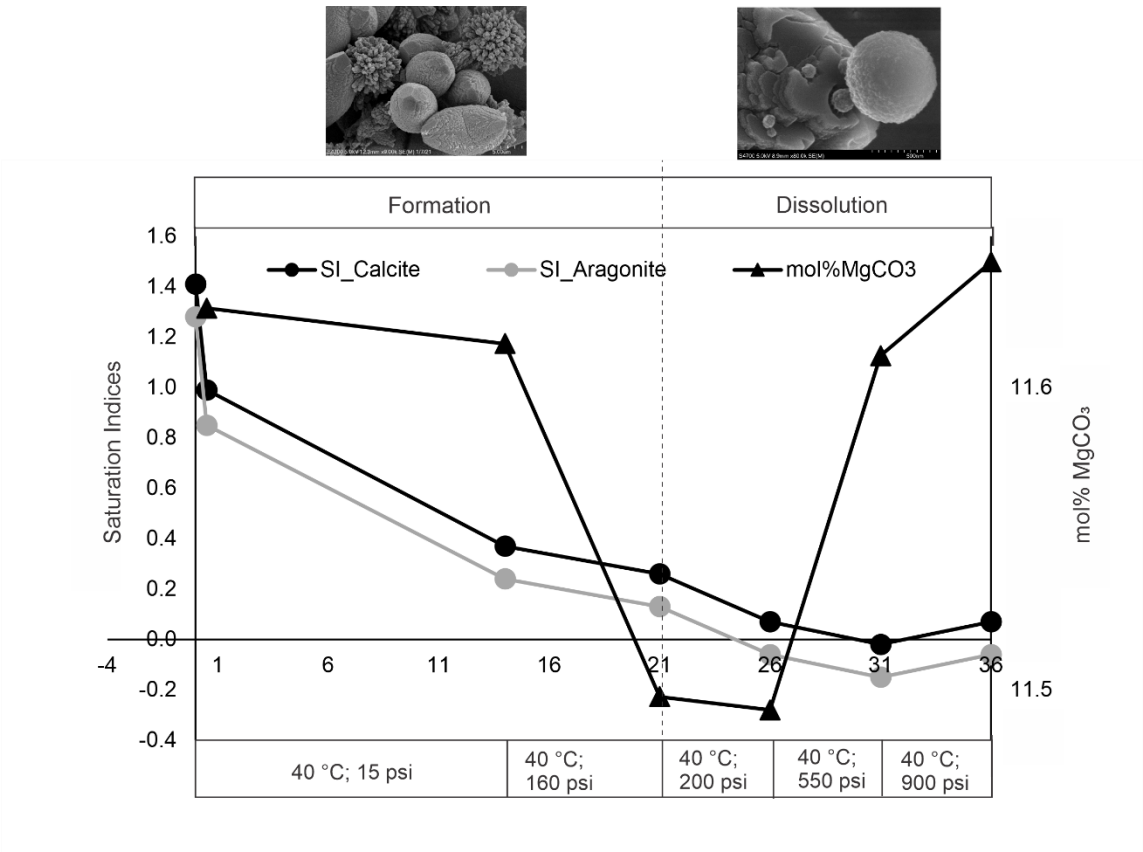

Figure 24 Schematic of pressure's effect on calcium carbonates

1) Formation

In control vessels, from day 0 to day 21, pH, alkalinity, concentrations of Mg^{2+} and Ca^{2+}, SIs of calcite and aragonite decreased, indicating carbonate mineral precipitation. The slight increase in fluid Mg:Ca ratio reflects that Ca was incorporated differentially into the solids compared to Mg, because Mg fits only into the calcite crystal lattice, while Ca is in both calcite and aragonite. Saturation indices decreased but remained above 0, indicating that calcium carbonates continued to precipitate. Although pressure was increased from 15 psi to 160 psi at day 14, the parameters (pH, alkalinity, fluid Mg:Ca ratio, saturation indices) showed little to no change. Results suggest that the increase in pressure was too slight to change mineral solubility, which is consistent with Phreeqc modeling results (Table 2).

2) Dissolution (Saturation indices < 0)

From day 21 to day 36, the pressure was increased to 200 psi for 5 days, then 550 psi for 5 days, and 900 psi for another 5 days. Commensurate with these changes in pressure there were increases in concentrations of Mg^{2+} and Ca^{2+}, but decreases in fluid Mg:Ca ratio and saturation indices of calcite and aragonite, which dropped below 0, signifying undersaturated conditions. It was noticed that the SIs slightly increased after day 31(900 psi), which was an experimental artifact caused by the quick removal of $CO_{2(g)}$ in the system when purging with $N_{2(g)}$ to generate high pressure. Without this experimental influence, SIs were expected to continue to decline. These conditions indicate dissolution of calcium carbonates, which is supported by noticeable changes in the morphology of COM-associated precipitates, with previously sharp edges becoming etched and embayed possibly due to dissolution (Figure 17b).

As shown in Table 2 and formula 2, while the pressure increases, all carbonate mineral saturation indices decrease but K_{sp}s increase, which correlate with slight increases in mol%$MgCO_3$.

These results are consistent with other lab results demonstrating that the solubility of Mg-calcite increases with increasing amount of Mg^{2+} entering the calcite lattice (Bischoff et al., 1993; Davis, 2000). Furthermore, it may indicate that magnesian calcites with higher solubility (more Mg) serve as a more stable phase in the new higher-pressure environment. It is inferred that the change of pressure drives the change in minerology, especially the change of mol%$MgCO_3$ in Mg-calcite. However, it is acknowledged that the minor changes in mol%$MgCO_3$ could be within experimental error (Figure 24).

Table 2 Solubilities of carbonate minerals, calculated by Phreeqc

T (°C)	P (psi)	ca depth (m)	Log (K_{sp}_Dolomite*)	Log (K_{sp}_Calcite*)	Log (K_{sp}_Aragonite*)
40	160	N/A	-17.4	-8.57	-8.44
40	200	N/A	-17.4	-8.57	-8.43
40	550	N/A	-17.36	-8.55	-8.41
40	900	N/A	-17.32	-8.52	-8.39
40	14.7	0	-17.42	-8.58	-8.45
40	100	30	-17.41	-8.57	-8.44
41	160	50	-17.42	-8.58	-8.45
47	900	300	-17.46	-8.58	-8.46

** The K_{sp} values of dolomite, calcite and aragonite (Plummer and Busenberg, 1982; Sherman and Barak, 2000)*

To sum up, early in burial history, dissolution is controlled by the thermodynamic adjustment of unstable phases like magnesian calcite and aragonite, which is one of the important porosity generation and permeability modification processes in carbonate rocks (Moore and Wade, 2013). The dissolution of metastable phases like Mg-calcite and aragonite help increase reservoir property, whereas the subsequent formation of calcite and/or dolomite can fill porosity and decrease permeability.

Experimentally simulated Diagenesis

The experiments in this study were adjusted to approximate the composition of Silurian seawater in a typical carbonate platform whose temperature gradient is 2.5 °C/100 m, and pressure gradient is 2.95 psi m^{-1} (Nwozor and Yardley, 2015). The chemistry of the fluid, mineralogy of precursor sediment, and chemical reactions caused by the change of pressure and temperature are determinants of diagenesis (Morse and Mackenzie, 1990; Higgins et al., 2018). In experiments in this study, the initial fluid chemistry was controlled (e.g. Silurian seawater), and pressure and temperature varied. Homogeneously precipitated mineral phases as well as the layered precipitates that are suspected to have formed heterogeneously on surfaces will both be affected by the increasing pressure and temperature after burial. Carbonates have retrograde solubility at high temperature, but solubility increases at high pressure, which is consistent with Phreeqc modeling results. Saturation indices slightly decrease with increasing pressure, but increase with increasing temperature (T < 65°C) (Figure 23). In the environment, the saturation indices of minerals are the aggregated effect of temperature and pressure. Therefore, the predominant factors in physical diagenesis, temperature or pressure, could be determined through the changing trend of saturation indices.

Pressure enhances the K_{sp} of dolomite, calcite, and aragonite (Figure 23 and Table 2), which is consistent with former work (Plummer and Busenberg, 1982; Sherman and Barak, 2000), but temperature reduces them in the temperature range below 65°C. In shallow burial environments (< 30 m), pressure controls the carbonate solubility at this burial depth, thus the saturation indices of carbonates slightly decrease (K_{sp}s increase) accordingly. However, after the pressure increases, indicative of deeper burial, the saturation indices of carbonates increase (K_{sp}s decrease), which means temperature becomes the predominant factor that controls the solubility

of carbonates in deeper burial environments. Mineral solubilities are reduced in general during diagenesis, tending to form low-Mg calcite and dolomite (Bischoff et al., 1993; Moore and Wade, 2013). This is consistent with the decrease of %mol $MgCO_3$ in experiments in this study, indicating transformation from high Mg-calcite to low Mg-calcite (%mol $MgCO_3$ < 4%), which correlates with changes in mineral solubilities calculated by Phreeqc. Experiments in this study demonstrate three processes. Other than two processes (formation and dissolution) which are the same as simulated-rapid diagenesis, one new process following by dissolution is reprecipitation.

Phase 3: reprecipitation

Carbonate saturation indices sharply increased after day 98 (47 °C, 900 psi), and metal ions in solutions decreased congruently, indicating the precipitation of calcium carbonate. Additionally, the mol% $MgCO_3$ decreased slightly, which means the K_{sp} of Mg-calcite decreased to fit in the higher-temperature environment. In addition, reprecipitation of aragonite and calcite were also observed under SEM, justifying the interpretation that there was regrowth of minerals (Figure 25).

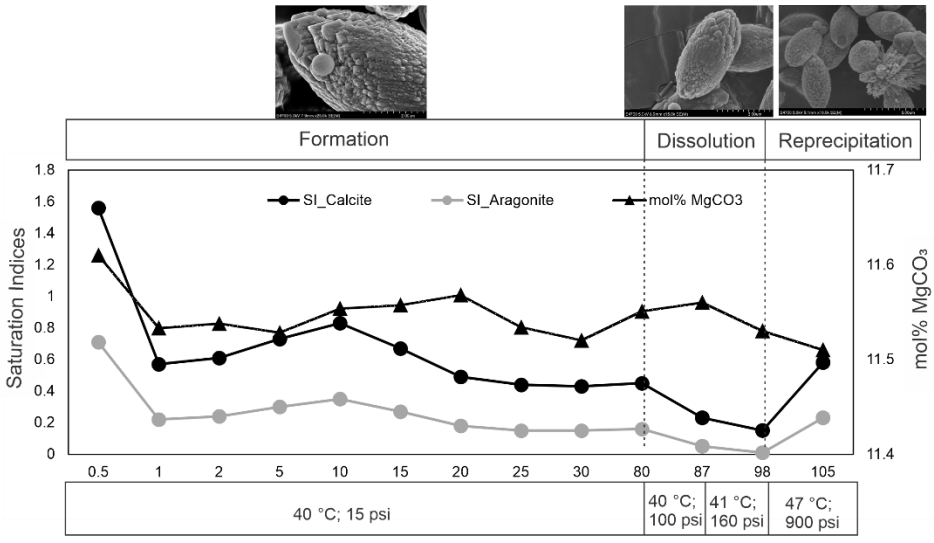

Figure 25 Schematic of experimentally-simulated diagenesis

In experimentally simulated diagenesis, the processes observed are formation of carbonate, dissolution, and finally reprecipitation based on the exchange of ions between solids and fluids, as evidence by changes fluid geochemistry, changes in %mol $MgCO_3$, and morphology of minerals under SEM. Similarly, in ancient sediments, diagenesis in carbonate rocks is usually followed by the dissolution of metastable minerals like aragonite and Mg-calcite, and the reprecipitation of calcite and dolomite (Moore and Wade, 2013).

Calcium carbonate precipitated from artificial Silurian seawater is a pH, alkalinity, fluid Mg:Ca ratio, and SI-reducing process. The increase of pressure tends to dissolve unstable precipitates and is more tolerant to calcite with higher Mg content (higher solubility), while the increase of temperature has the opposite effect. Pressure is the dominant factor in rapid burial diagenesis, and minerals with higher solubility is a stable form. In contrast, temperature dominates the normal diagenesis, at which the metastable carbonates transform to low-Mg or low-solubility form.

Implications

Results from this study supports previous studies that implicate COM in the formation of low-temperature dolomite. Although dolomite was not detected, the accumulation of Mg on COM surfaces, suggest that with longer incubation times, Mg-rich Ca carbonates may have formed. While temperature and pressure impact carbonate equilibria and with it $MgCO_3$% of calcite, the largest impact in Mg-content is likely on the surface of COM. In environments ranging from surface to shallow subsurface, sediments contain microorganisms and other forms of organic matter, clay minerals, and in some anoxic environments, dissolved sulfide and CH_4, all of which can facilitate Mg-rich carbonate formation under conditions that are supersaturated with respect to dolomite. Many studies have observed that Mg-rich calcites recrystallize to dolomite with burial. The experiments in this study did not capture this process despite incubation with increased pressure. It is hypothesized that there are several reasons for this outcome. One reason may be that the initial nucleation phase did not produce VHMC, which is a necessary precursor. Previous studies have shown that the density of carboxyl groups on organic matter play a role in dolomite nucleation (Kenward et al., 2013). While COM in this study was similar to that used by Roberts et al. (2013) the batches were different and may not have had the density of carboxyl groups necessary for dolomite nucleation. Another possibility is the fact that experiments were performed in batch. Had flow-through conditions been present, sustained saturated conditions may contribute to recrystallization and dolomite formation. Finally, it is likely that the short time frame of these experiments was unable to capture recrystallization processes despite the changes in pressure that were applied. All of these issues give insight into additional work that can address these issues and further elucidate controls on formation of dolomite in low temperature environments.

References

Arndt Nicholas (2011) Geothermal Gradient. In *Encyclopedia of Astrobiology* (eds. M. Gargaud, R. Amils, J. C. Quintanilla, H. J. (Jim) Cleaves, W. M. Irvine, D. L. Pinti, and M. Viso). Springer, Berlin, Heidelberg. pp. 662–662.

Arvidson R. S. and Mackenzie Fred T (1999) The dolomite problem; control of precipitation kinetics by temperature and saturation state. *American Journal of Science* **299**, 257–288.

Bischoff William D., Bertram Miriam A., Mackenzie Fred T. and Bishop Finley C. (1993) Diagenetic stabilization pathways of magnesian calcites. *Carbonates Evaporites* **8**, 82–89.

Bontognali Tomaso R. R., Vasconcelos Crisógono, Warthmann Rolf J., Bernasconi Stefano M., Dupraz Christophe, Strohmenger Christian J. and McKENZIE Judith A. (2010) Dolomite formation within microbial mats in the coastal sabkha of Abu Dhabi (United Arab Emirates). *Sedimentology* **57**, 824–844.

Braissant O., Decho A. W., Dupraz C., Glunk C., Przekop K. M. and Visscher P. T. (2007) Exopolymeric substances of sulfate-reducing bacteria: Interactions with calcium at alkaline pH and implication for formation of carbonate minerals. *Geobiology* **5**, 401–411.

Braithwaite Cjr (1991) Dolomites, a Review of Origins, Geometry and Textures. *Trans. R. Soc. Edinb.-Earth Sci.* **82**, 99–112.

Brennan Sean T and Lowenstein Tim K (2002) The major-ion composition of silurian seawater. *Geochimica et Cosmochimica Acta* **66**, 2683–2700.

Brezonik Patrick L and Arnold William A (2011) *Water chemistry: an introduction to the chemistry of natural and engineered aquatic systems*., Oxford University Press, New York.

Davis K. J. (2000) The Role of Mg^{2+} as an Impurity in Calcite Growth. *Science* **290**, 1134–1137.

De Choudens-Sanchez Vionette (2007) Calcium carbonate polymorphism: New insights into the role of solution saturation state and composition (magnesium/calcium) on calcium carbonate mineralogy, morphology and fabrics. Doctoral thesis, University of Kansas.

Dickson J.A.D. (2004) Echinoderm Skeletal Preservation: Calcite-Aragonite Seas and the Mg/Ca Ratio of Phanerozoic Oceans. *Journal of Sedimentary Research* **74**, 355–365.

Dix George R. and Mullins Henry T. (1988) Rapid burial diagenesis of deep-water carbonates: Exuma Sound, Bahamas. *Geology* **16**, 680–683.

Freeze Allan and Cherry John (1979) Groundwater. In Prentice-Hall, Englewood Cliffs, N.J. p. 97.

Gabellone Tatyana and Whitaker Fiona (2016) Secular variations in seawater chemistry controlling dolomitization in shallow reflux systems: insights from reactive transport modelling ed. G. Della Porta. *Sedimentology* **63**, 1233–1259.

Hacker Bradley R., Rubie David C., Kirby Stephen H. and Bohlen Steven R. (2005) The calcite → aragonite transformation in low-Mg marble: Equilibrium relations, transformation mechanisms, and rates. *Journal of Geophysical Research: Solid Earth* **110**.

Higgins J.A., Blättler C.L., Lundstrom E.A., Santiago-Ramos D.P., Akhtar A.A., Crüger Ahm A-S., Bialik O., Holmden C., Bradbury H., Murray S.T. and Swart P.K. (2018) Mineralogy, early marine diagenesis, and the chemistry of shallow-water carbonate sediments. *Geochimica et Cosmochimica Acta* **220**, 512–534.

Holland Heinrich D., Lazar B. and McCaffrey M. (1986) Evolution of the atmosphere and oceans. *Nature* **320**, 27–33.

Kaczmarek Stephen E., Gregg Jay M., Bish David L., Machel Hans G. and Fouke Bruce W. (2017) Dolomite, very high-magnesium calcite, and microbes—implications for the microbial model of dolomitization. In *Characterization and Modeling of Carbonates–Mountjoy Symposium 1* SEPM (Society for Sedimentary Geology).

Kaczmarek Stephen E. and Sibley Duncan F. (2014) Direct physical evidence of dolomite recrystallization ed. A. Immenhauser. *Sedimentology* **61**, 1862–1882.

Kaczmarek Stephen E. and Sibley Duncan F. (2011) On the evolution of dolomite stoichiometry and cation order during high-temperature synthesis experiments: An alternative model for the geochemical evolution of natural dolomites. *Sediment. Geol.* **240**, 30–40.

Kaczmarek Stephen E. and Thornton Brian P. (2017) The effect of temperature on stoichiometry, cation ordering, and reaction rate in high-temperature dolomitization experiments. *Chemical Geology* **468**, 32–41.

Kaczmarek Stephen E., Whitaker Fiona F., Avila Mike, Lewis David and Saccocia Peter J. (2019) A Case for Caution When Using Geochemical Models to Make Predictions About Dolomite. In AAPG Annual Convention and Exhibition.

Kawano Jun, Shimobayashi Norimasa, Miyake Akira and Kitamura Masao (2009) Precipitation diagram of calcium carbonate polymorphs: its construction and significance. *J. Phys.: Condens. Matter* **21**, 425102.

Kenward Paul A., Fowle David A., Goldstein Robert H., Ueshima Masato, González Luis A. and Roberts Jennifer A. (2013) Ordered low-temperature dolomite mediated by carboxyl-group density of microbial cell walls. *Bulletin* **97**, 2113–2125.

Li Mingtao, Wignall Paul B., Dai Xu, Hu Mingyi and Song Haijun (2021) Phanerozoic variation in dolomite abundance linked to oceanic anoxia. *Geology* **49**, 698–702.

Lippmann Friedrich (1973) The System CaCO3-MgCO3. In *Sedimentary Carbonate Minerals* (ed. F. Lippmann). Minerals, Rocks and Inorganic Materials. Springer, Berlin, Heidelberg. pp. 148–190.

Liu Deng, Xu Yangyang, Papineau Dominic, Yu Na, Fan Qigao, Qiu Xuan and Wang Hongmei (2019) Experimental evidence for abiotic formation of low-temperature proto-dolomite facilitated by clay minerals. *Geochimica et Cosmochimica Acta* **247**, 83–95.

Lowenstein Tim K., Timofeeff Michael N., Brennan Sean T., Hardie Lawrence A. and Demicco Robert V. (2001) Oscillations in Phanerozoic Seawater Chemistry: Evidence from Fluid Inclusions. *Science* **294**, 1086–1088.

Lu Yang, Sun Xiaoming, Xu Huifang, Konishi Hiromi, Lin Zhiyong, Xu Li, Chen Tingting, Hao Xinrong, Lu Hongfeng and Peckmann Jörn (2018) Formation of dolomite catalyzed by sulfate-driven anaerobic oxidation of methane: Mineralogical and geochemical evidence from the northern South China Sea. *American Mineralogist* **103**, 720–734.

Manche Cameron J. and Kaczmarek Stephen E. (2021) A global study of dolomite stoichiometry and cation ordering through the Phanerozoic. *Journal of Sedimentary Research* **91**, 520–546.

Mirsal Ibrahim A. and Zankl Heinrich (1985) Some phenomenological aspects of carbonate geochemistry. The control effect of transition metals. *Geol Rundsch* **74**, 367–377.

Moore Clyde H. and Wade William J. (2013) *Carbonate Reservoirs: Porosity and Diagenesis in a Sequence Stratigraphic Framework.*, Newnes.

Morse John W. and Mackenzie Fred T. editors (1990) Chapter 8 Carbonates as Sedimentary Rocks in Subsurface Processes. In *Developments in Sedimentology* Geochemistry of Sedimentary Carbonates. Elsevier. pp. 373–446.

Nwozor Kingsley and Yardley Gareth (2015) Overburden Stress Estimation: A New Model for the UK Sector of the Central North Sea. In AAPG/SEG International Conference & Exhibition. Melbourne, Australia. p. 14.

Parkhurst David L. and Appelo C.A.J. (1999) *User's guide to PHREEQC (Version 2): A computer program for speciation, batch-reaction, one-dimensional transport, and inverse geochemical calculations*., U.S. Geological Survey.

Petrash Daniel A., Bialik Or M., Bontognali Tomaso R.R., Vasconcelos Crisógono, Roberts Jennifer A., McKenzie Judith A. and Konhauser Kurt O. (2017) Microbially catalyzed dolomite formation: From near-surface to burial. *Earth-Science Reviews* **171**, 558–582.

Plummer L. Niel and Busenberg Eurybiades (1982) The solubilities of calcite, aragonite and vaterite in CO2-H2O solutions between 0 and 90°C, and an evaluation of the aqueous model for the system CaCO3-CO2-H2O. *Geochimica et Cosmochimica Acta* **46**, 1011–1040.

Qiu Xuan, Wang Hongmei, Yao Yanchen and Duan Yong (2017) High salinity facilitates dolomite precipitation mediated by Haloferax volcanii DS52. *Earth and Planetary Science Letters* **472**, 197–205.

Qiu Xuan, Yao Yancheng, Wang Hongmei, Shen Anjiang and Zhang Jie (2019) Halophilic Archaea Mediate the Formation of Proto-Dolomite in Solutions With Various Sulfate Concentrations and Salinities. *Front. Microbiol.* **10**, 480.

Ren Min and Jones Brian (2018) Genesis of island dolostones ed. P. Pufahl. *Sedimentology* **65**, 2003–2033.

Roberts Jennifer A., Bennett Philip C., González Luis A., Macpherson G.L. and Milliken Kitty L. (2004) Microbial precipitation of dolomite in methanogenic groundwater. *Geol* **32**, 277.

Roberts Jennifer A., Kenward Paul A., Fowle David A., Goldstein Robert H., González Luis A. and Moore David S. (2013) Surface chemistry allows for abiotic precipitation of dolomite at low temperature. *Proc Natl Acad Sci USA* **110**, 14540–14545.

Romanek Christopher S., Jiménez-López Concepción, Navarro Alejandro Rodriguez, Sánchez-Román Monica, Sahai Nita and Coleman Max (2009) Inorganic synthesis of Fe–Ca–Mg carbonates at low temperature. *Geochimica et Cosmochimica Acta* **73**, 5361–5376.

Ryan Brooks H., Kaczmarek Stephen E. and Rivers John M. (2020) Early and pervasive dolomitization by near-normal marine fluids: New lessons from an Eocene evaporative setting in Qatar. *Sedimentology*, sed.12726.

Sánchez-Román Mónica, Vasconcelos Crisógono, Schmid Thomas, Dittrich Maria, McKenzie Judith A., Zenobi Renato and Rivadeneyra Maria A. (2008) Aerobic microbial dolomite at the nanometer scale: Implications for the geologic record. *Geol* **36**, 879.

Shen Zhizhang, Liu Yun, Brown Philip E., Szlufarska Izabela and Xu Huifang (2014) Modeling the Effect of Dissolved Hydrogen Sulfide on Mg^{2+} –Water Complex on Dolomite {104} Surfaces. *J. Phys. Chem. C* **118**, 15716–15722.

Sherman Leslie A. and Barak Phillip (2000) Solubility and Dissolution Kinetics of Dolomite in Ca–Mg–HCO3/CO3 Solutions at 25°C and 0.1 MPa Carbon Dioxide. *Soil Science Society of America Journal* **64**, 1959–1968.

Shinn Eugene A. and Ginsburg R. N. (1964) Formation of Recent Dolomite in Florida and the Bahamas: ABSTRACT. *AAPG Bulletin* **48**, 547–547.

Tucker Maurice E. and Wright V. Paul (1990) *Carbonate Sedimentology*., Blackwell Scientific Publications, Boston.

Vasconcelos Crisogono and McKenzie Judith A. (1997) Microbial mediation of modern dolomite precipitation and diagenesis under anoxic conditions (Lagoa Vermelha, Rio de Janeiro, Brazil). *Journal of Sedimentary Research* **67**, 378–390.

Warren John (2000) Dolomite: occurrence, evolution and economically important associations. *Earth-Science Reviews* **52**, 1–81.

Wright David T. and Wacey David (2005) Precipitation of dolomite using sulphate-reducing bacteria from the Coorong Region, South Australia: significance and implications. *Sedimentology* **52**, 987–1008.

Zhang Fangfu, Xu Huifang, Konishi Hiromi, Kemp Joshua M., Roden Eric E. and Shen Zhizhang (2012) Dissolved sulfide-catalyzed precipitation of disordered dolomite: Implications for the formation mechanism of sedimentary dolomite. *Geochimica et Cosmochimica Acta* **97**, 148–165.

Zhang Fangfu, Xu Huifang, Konishi Hiromi, Shelobolina Evgenya S. Shelobolina and Roden Eric E. (2012) Polysaccharide-catalyzed nucleation and growth of disordered dolomite: A potential precursor of sedimentary dolomite. *American Mineralogist* **97**, 556–567.